Supporting Information

for

Spectral and Electronic Properties of Nitrosylcobalamin

Ivan G. Pallares and Thomas C. Brunold

NOCbl Synthesis: For the preparation of pure NO gas, small amounts (<1 mg) of copper tetrachloride ($CuCl_4$), ascorbic acid, and sodium nitrite ($NaNO_3$) were dissolved in 500 µL of degassed MilliQ water in a vial purged with Argon gas. The reaction was allowed to proceed for 1 minute. Under positive argon pressure, a steel cannula that was connected to the vial containing the NO gas was inserted into a freshly prepared ~2 mM Co(II)Cbl solution (see main text for details). A distinct color change from yellow to orange was observed upon the reaction of Co(II)Cbl with NO gas. The reaction was allowed to proceed for 2 hours at room temperature before the cannula was removed and the headspace of the vial containing the NOCbl product was purged with argon for 5 minutes. Following this preparation, spectroscopic samples were prepared according to the methods outlined previously.[1]

Calculation of effective number of d-electrons: From the NBO composition of each Co-based NLMO, the effective number of Co 3d electrons can be estimated as follows. [2] First, the electrons in the Co-based NLMOs are partitioned into formally occupied (high occupancy) and empty (low-occupancy) NBOs.

$$\varphi_{NLMO} = \alpha \cdot \phi_{high-occ} + (1-\alpha) \cdot \phi_{low-occ} \qquad (1)$$

Where α is the fractional contribution from the Co-based NBOs, obtained from the %NBO character computed for the corresponding NLMO. To obtain the Co 3d AO contributions to each NBOs, the %Co and %N compositions from our NBO analysis were used.

$$\phi_{high-occ} = \delta \cdot \chi_{Co} + (1 - \delta) \cdot \chi_{non-Co} \quad (2)$$

Where δ is the fractional contribution from Co-based orbitals (see Table 5). To estimate the fractional number of 3d electrons, *d*, the contributions from the Co 3d AOs to each doubly-occupied Co-based NLMO obtained by the product of δ and α are weighted by the occupancy of the NLMO.

$$d = \sum_{NLMOs} 2 \cdot \alpha_i.\delta_i \quad (3)$$

For the case where the NLMOs are singly occupied, a sum for each spin manifold is carried out.

$$d = \sum_{spin-up} 1 \cdot \alpha_i.\delta_i + \sum_{spin-down} 1 \cdot \alpha_i.\delta_i \quad (4)$$

Table S1: Compositions of selected canonical MOs of NOCbl (see Figure S13 for atom numbering scheme)

MO	Atom		AO	% Cont.	MO	Atom		AO	% Cont.	MO	Atom		AO	% Cont.
158	1	Co	dx2y2	85.4	162	1	Co	dyz	28.2	166	1	Co	dyz	2.6
159	1	Co	dxz	20.7		2	N	pz	8.1		2	N	pz	7.1
	1	Co	dx2y2	3.6		3	N	pz	3.4		5	N	pz	7.6
	42	N	px	7		10	C	pz	9		9	C	pz	4.5
	44	N	px	6.3		11	C	pz	5.7		10	C	pz	4.9
	45	C	px	17.6		14	C	pz	5.7		11	C	pz	6.4
	46	C	px	7.1		16	C	pz	7.9		14	C	pz	11.8
	48	C	px	16		19	C	pz	2.3		16	C	pz	12.7
	49	C	px	2.3		54	N	py	2.4		19	C	pz	8
160	1	Co	dxz	5.2		55	O	py	2.9		20	C	pz	4.4
	43	C	px	11.7	163	2	N	pz	3.1		21	C	pz	5.3
	46	C	px	19.5		3	N	pz	9.2	167	1	Co	dz2	7.6
	47	C	px	16		4	N	pz	11.5		1	Co	dxz	2.1
	49	C	px	15.6		5	N	pz	8.2		1	Co	dxy	32.1
	50	C	px	14.2		10	C	pz	8		2	N	px	3.4
161	1	Co	dz2	2		15	C	pz	14.9		3	N	pz	2.9
	1	Co	dxz	35.2		20	C	pz	15.7		4	N	py	2.1
	19	C	pz	2.5		44	N	pz	2.7		5	N	px	2.6
	42	N	px	3.5	164	1	Co	dz2	28.1		9	C	pz	3.5
	43	C	px	3.6		1	Co	dxz	12		11	C	pz	2.3
	44	N	px	4.8		44	N	pz	3.8		15	C	pz	2.4
	45	C	px	8.4		54	N	s	3.4		54	N	pz	4.8
	47	C	px	6.9		54	N	pz	7.7		55	O	pz	2.6
	48	C	px	9.2		54	N	px	10.3	168	53	Co	dz2	14.6
	50	C	px	2.6		55	O	pz	12.6		53	Co	dxy	21.2
	55	O	pz	3.7		55	O	px	8.7		53	N	pz	3.5
					165	1	Co	dyz	14.8		53	C	pz	2.1
						54	N	py	47.7		53	C	pz	2.5
						55	O	py	30.6		53	C	pz	2.1
											53	C	pz	3.8
											53	N	pz	9.9
											53	O	pz	5

Table S2: Compositions of selected canonical MOs of $NOCbi^+$ (see Figure S13 for atom numbering scheme)

MO	Atom		AO	% Cont.	MO	Atom		AO	% Cont.	MO	Atom		AO	% Cont.
126	1	Co	dx2y2	88.8	129	1	Co	dz2	2.3	132	1	Co	dyz	3.6
127	1	Co	dz2	23.1		1	Co	dyz	20.5		1	Co	dxy	2.1
	1	Co	dxz	16.1		2	N	pz	2.8		2	N	pz	7.4
	1	Co	dyz	2.5		4	N	pz	2.6		5	N	pz	7.2
	3	N	pz	4.3		5	N	pz	8.8		9	C	pz	6.3
	4	N	pz	2.4		10	C	pz	2.2		10	C	pz	4.4
	9	C	pz	2.9		11	C	pz	2.6		11	C	pz	7.8
	10	C	pz	3		14	C	pz	7.5		14	C	pz	12.2
	15	C	pz	8.2		16	C	pz	5.8		16	C	pz	12
	21	C	pz	3.2		19	C	pz	7.1		19	C	pz	6.7
	45	N	pz	2		20	C	pz	10.3		20	C	pz	4.5
	45	N	px	3.9		45	N	py	2.7		21	C	pz	4.6
	46	O	pz	8.3		46	O	py	3.2	133	1	Co	pz	4.7
	46	O	px	3.5	130	1	Co	dz2	17		1	Co	dz2	20.5
128	1	Co	dxz	37.3		1	Co	dxz	20		1	Co	dxy	9.7
	2	N	pz	6.3		3	N	pz	3.9		3	N	pz	3
	3	N	pz	3.8		4	N	pz	3.5		15	C	pz	3.2
	4	N	pz	2.1		10	C	pz	3.6		45	N	pz	17.9
	5	N	pz	2.4		15	C	pz	4		45	N	px	5.2
	10	C	pz	9		20	C	pz	3.6		46	O	pz	10.5
	11	C	pz	5.9		45	N	s	3.1		46	O	px	2.5
	15	C	pz	4.3		45	N	pz	4.9	134	1	Co	dz2	7.1
	19	C	pz	2.4		45	N	px	7.4		1	Co	dxy	38.8
	20	C	pz	4		46	O	pz	7		2	N	px	2.3
	46	O	pz	2.2		46	O	px	6.1		3	N	px	2.3
					131	1	Co	dyz	16.4		3	N	py	2.1
						45	N	py	48		5	N	px	4.5
						46	O	py	30.4		14	C	pz	2.5
											45	N	pz	5.4
											46	O	pz	2.8

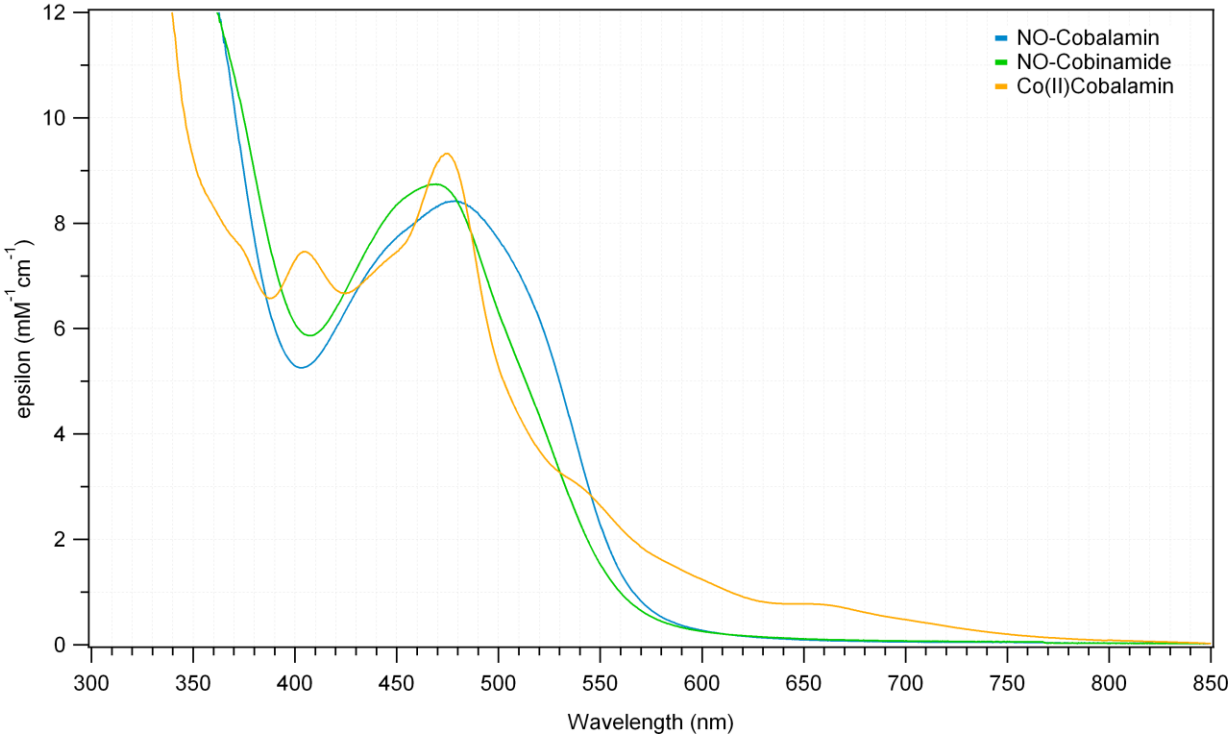

Figure S1: Abs spectra at 298 K of Co(II)Cbl and Co(II)Cbi$^+$ after exposure to NO gas overlayed with the Abs spectrum of Co(II)Cbl. The absence of features above 600 nm in the Abs spectra of NOCbl and NOCbi$^+$ indicates that the amount of unreacted Co(II) species is negligible.

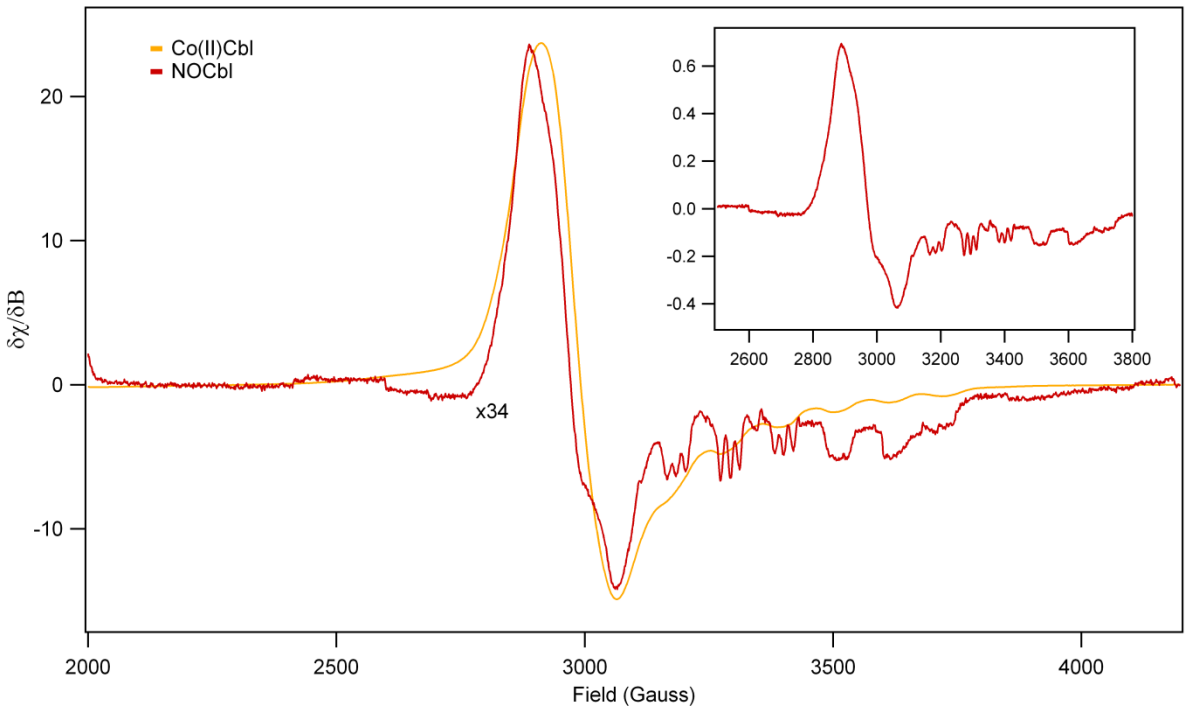

Figure S2: 40 K EPR spectra of Co(II)Cbl before (yellow) and after (red) exposure to NO gas. Because the red trace had to be magnified 34-fold to match the signal intensity of the yellow trace, it can be estimated that less than 3% of unreacted Co(II)Cbl remained in solution. Inset: unscaled EPR spectrum of NOCbl.

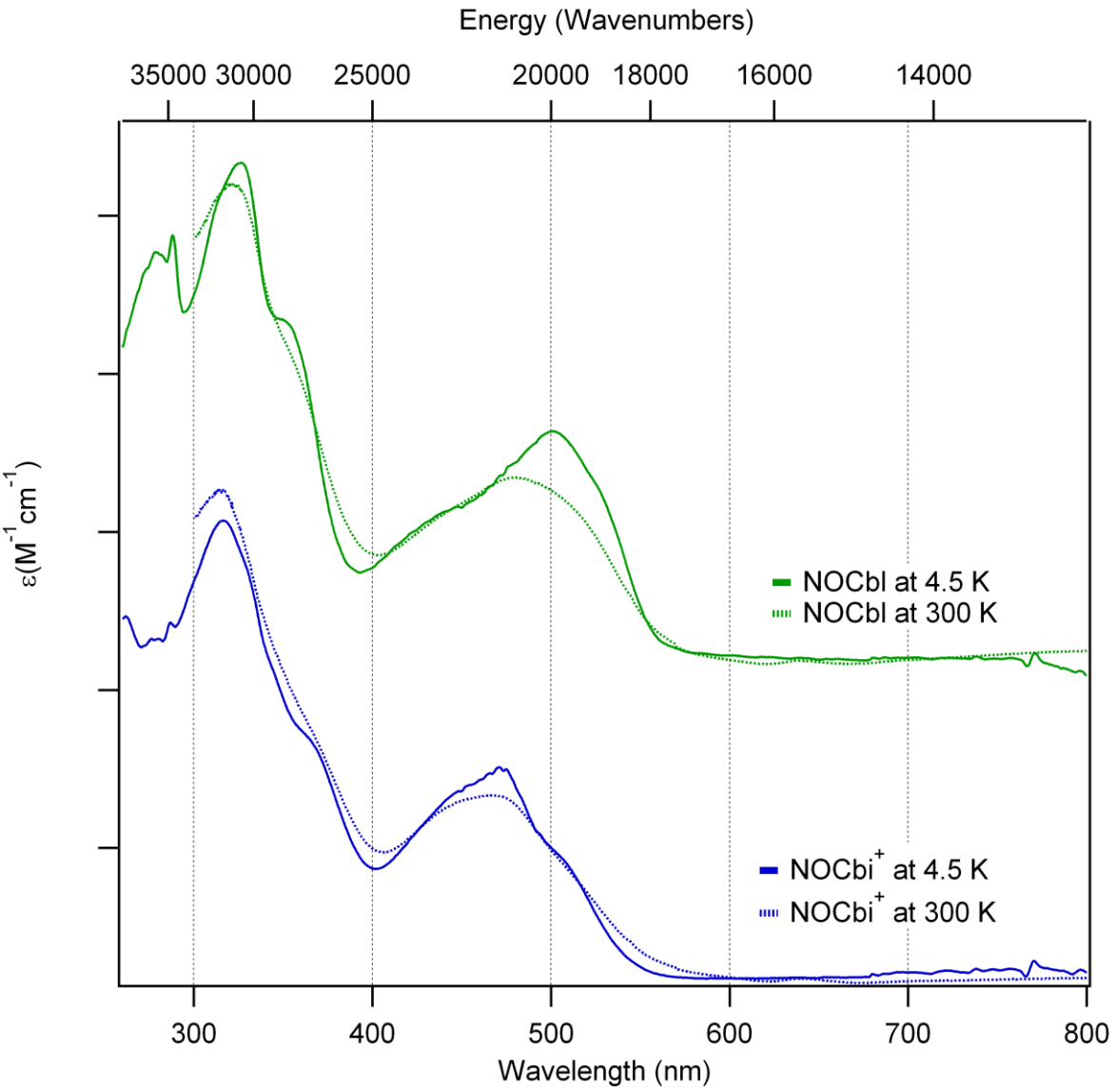

Figure S3: Abs spectra of NOCbl and $NOCbi^+$ at 4.5 K and 300 K in 60:40 (v:v) glycerol:water solution. The blue-shift of the α-band observed for NOCbl from 4.5 to 300 K reflects sizable changes in the Co(II) coordination environment. In contrast, the lack of a similar band shift observed for $NOCbi^+$ indicates that in this case the Co(II) coordination environment does not change as a function of temperature.

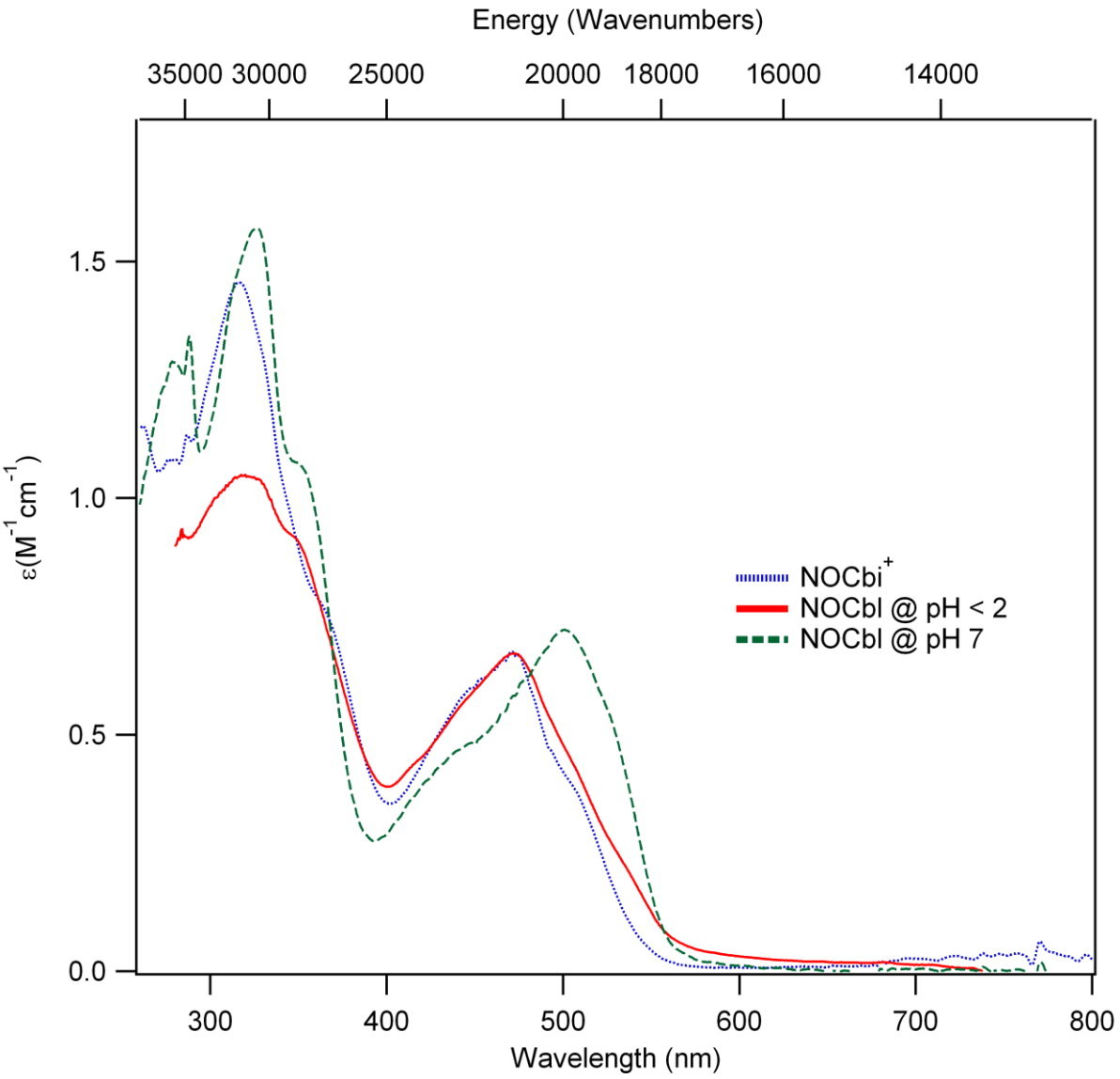

Figure S4: Abs spectra of NOCbl at pH < 2 and of NOCbl and $NOCbi^+$ at neutral pH, collected at 4.5 K in 60:40 (v:v) glycerol:water solution. At low pH, NOCbl is present predominantly in the base-off state, as shown by the blueshift of the α-band upon acidification and the similarity of the resulting spectrum with that of $NOCbi^+$.

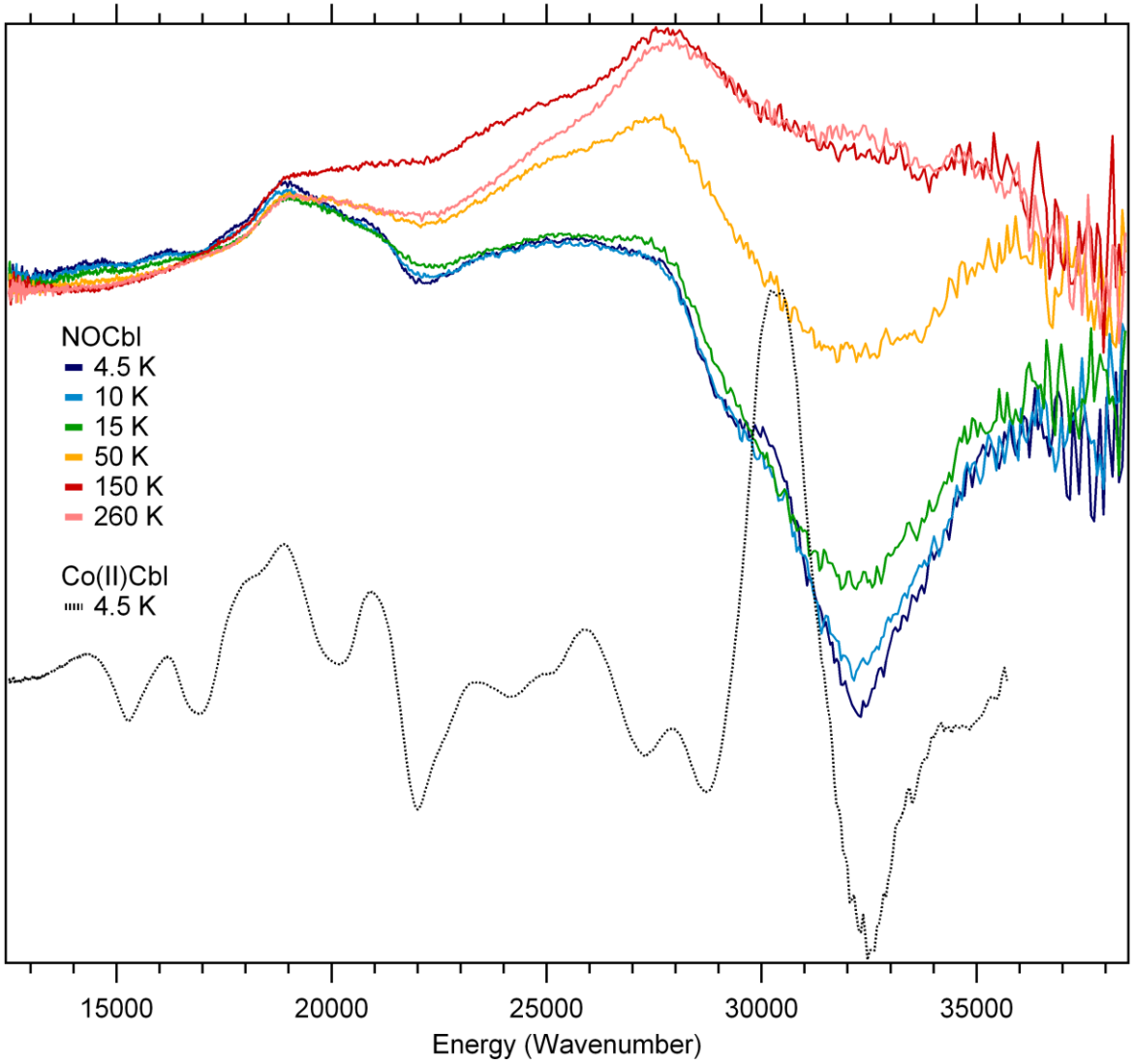

Figure S5: 7 T MCD spectra at various temperatures of NOCbl in the "base-on" state (top) traces and at 4.5 K of Co(II)Cbl. The minor temperature dependence of the features in the NOCbl spectra is due to changes in glass strain and band width as a function of temperature.

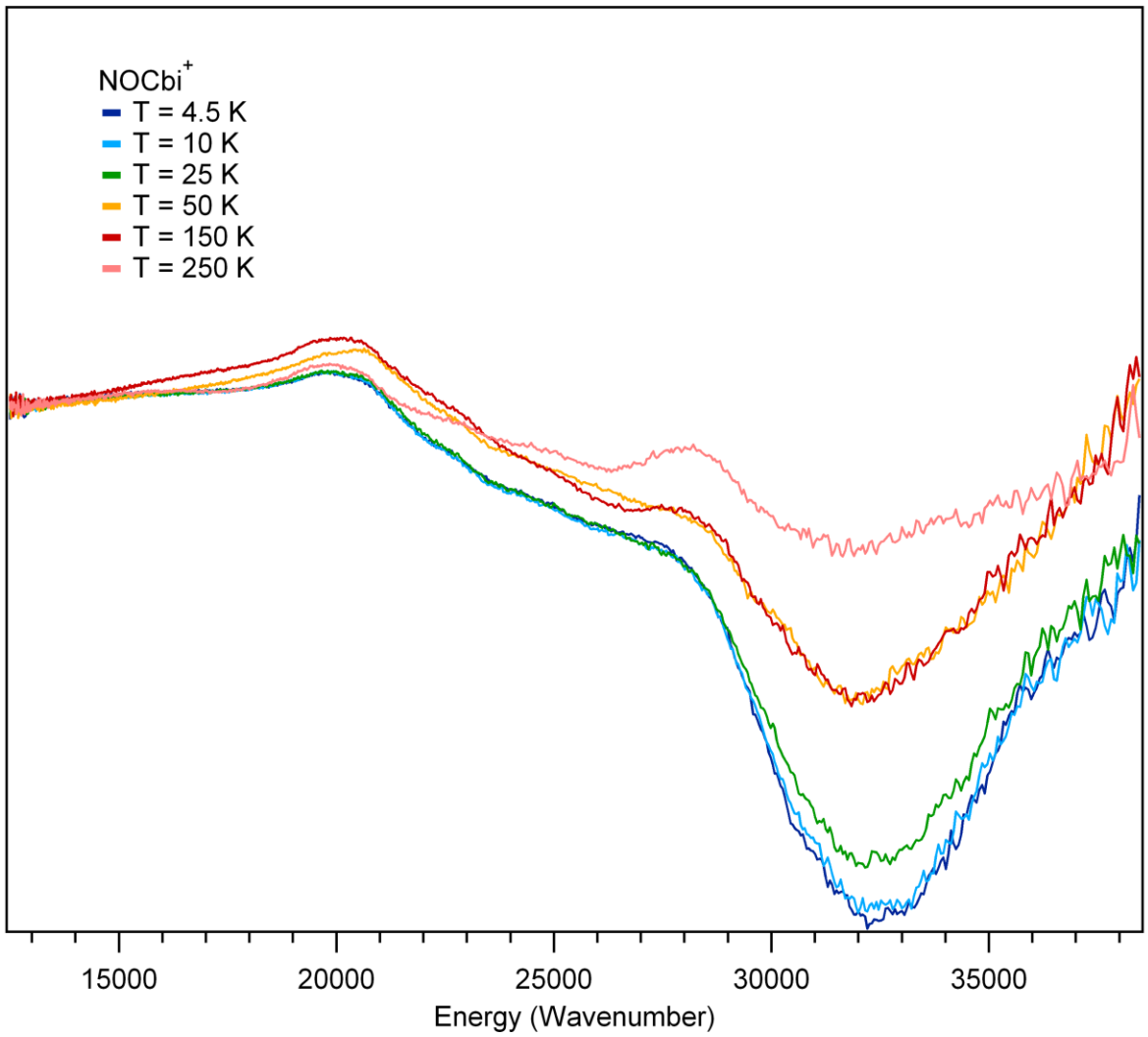

Figure S6: 7 T MCD spectra at various temperatures of $NOCbi^+$, a model of "base-off" NOCbl. The minor temperature dependence of the observed features is due to changes in glass strain and band width as a function of temperature.

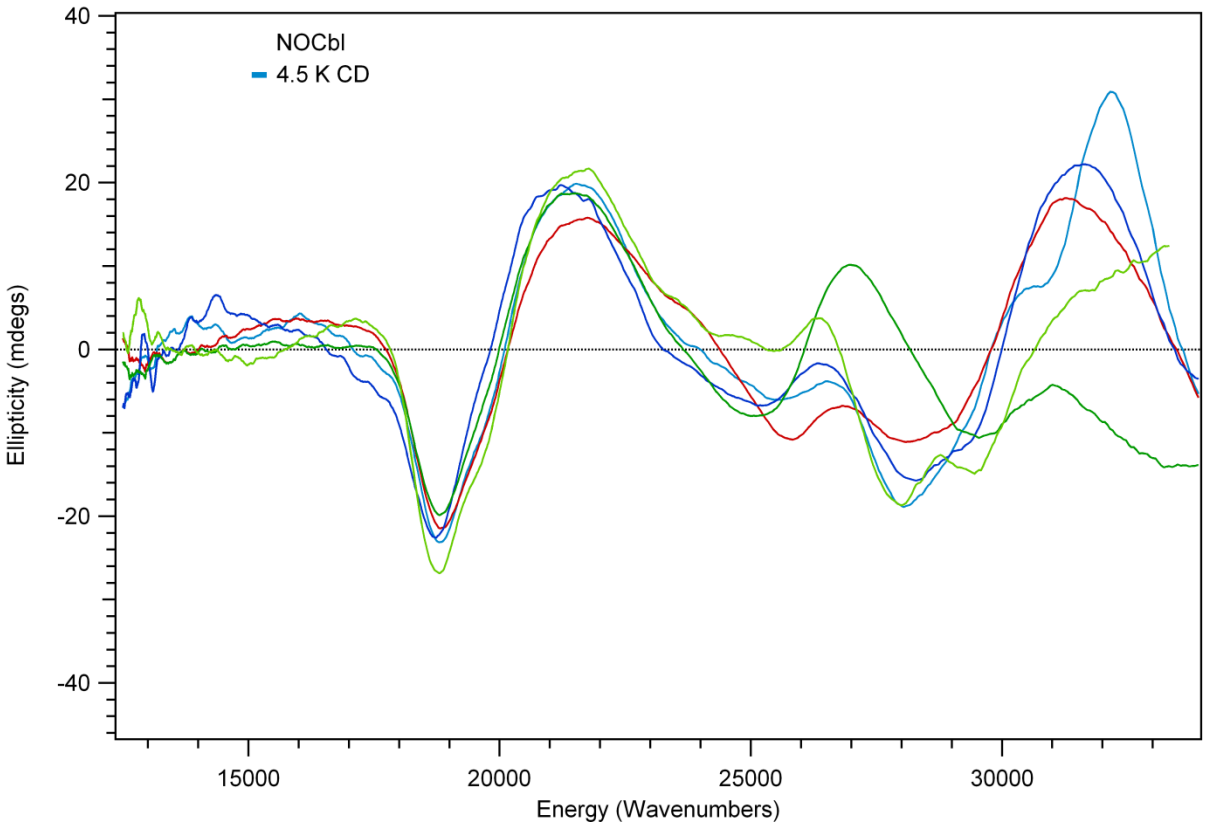

Figure S7: 4.5 K CD spectra of several independently prepared NOCbl samples. Although the CD features at higher energies are not fully reproducible, the predominant derivative-shaped feature at 19,000 cm^{-1} is consistently observed.

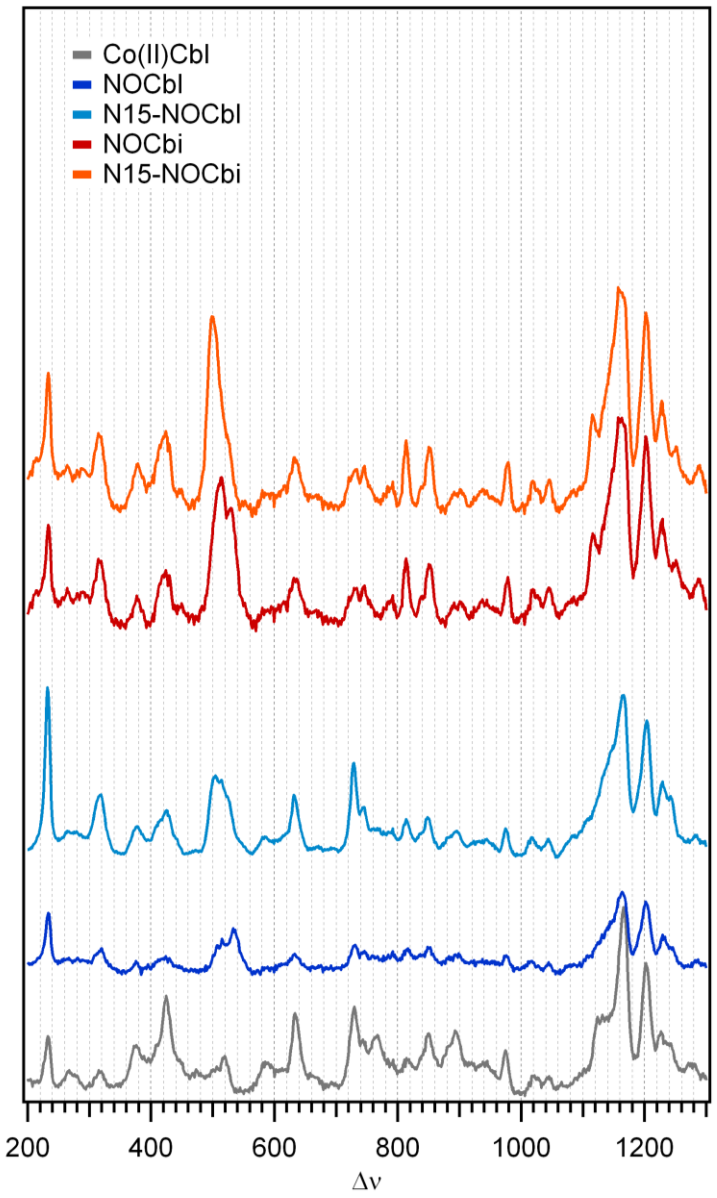

Figure S8: Low-energy region of rR spectra of Co(II)Cbl, NOCbl, and $NOCbi^{+}$ obtained at 77 K with 488 nm (20 491 cm^{-1}) laser excitation

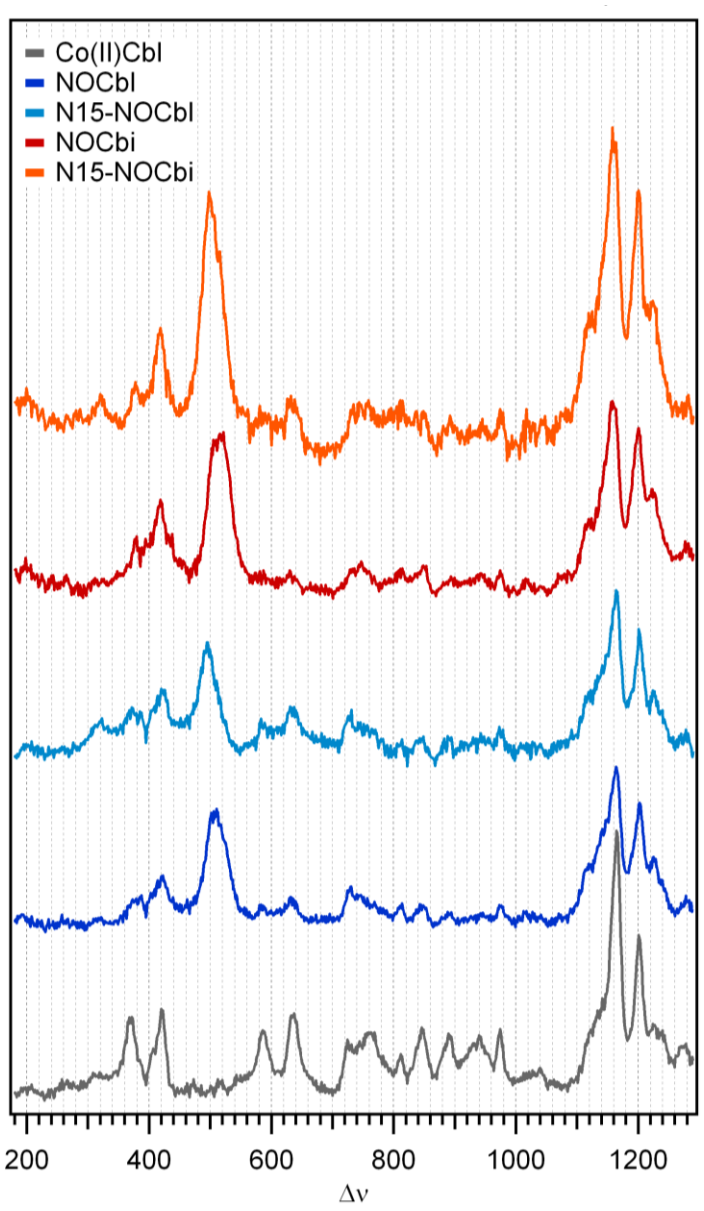

Figure S9: Low-energy region of rR spectra of Co(II)Cbl, NOCbl, and $NOCbi^{+}$ obtained at 278 K with 488 nm (20 491 cm^{-1}) laser excitation. Note that changes from the 77 K spectra can be attributed to band broadening at higher temperature.

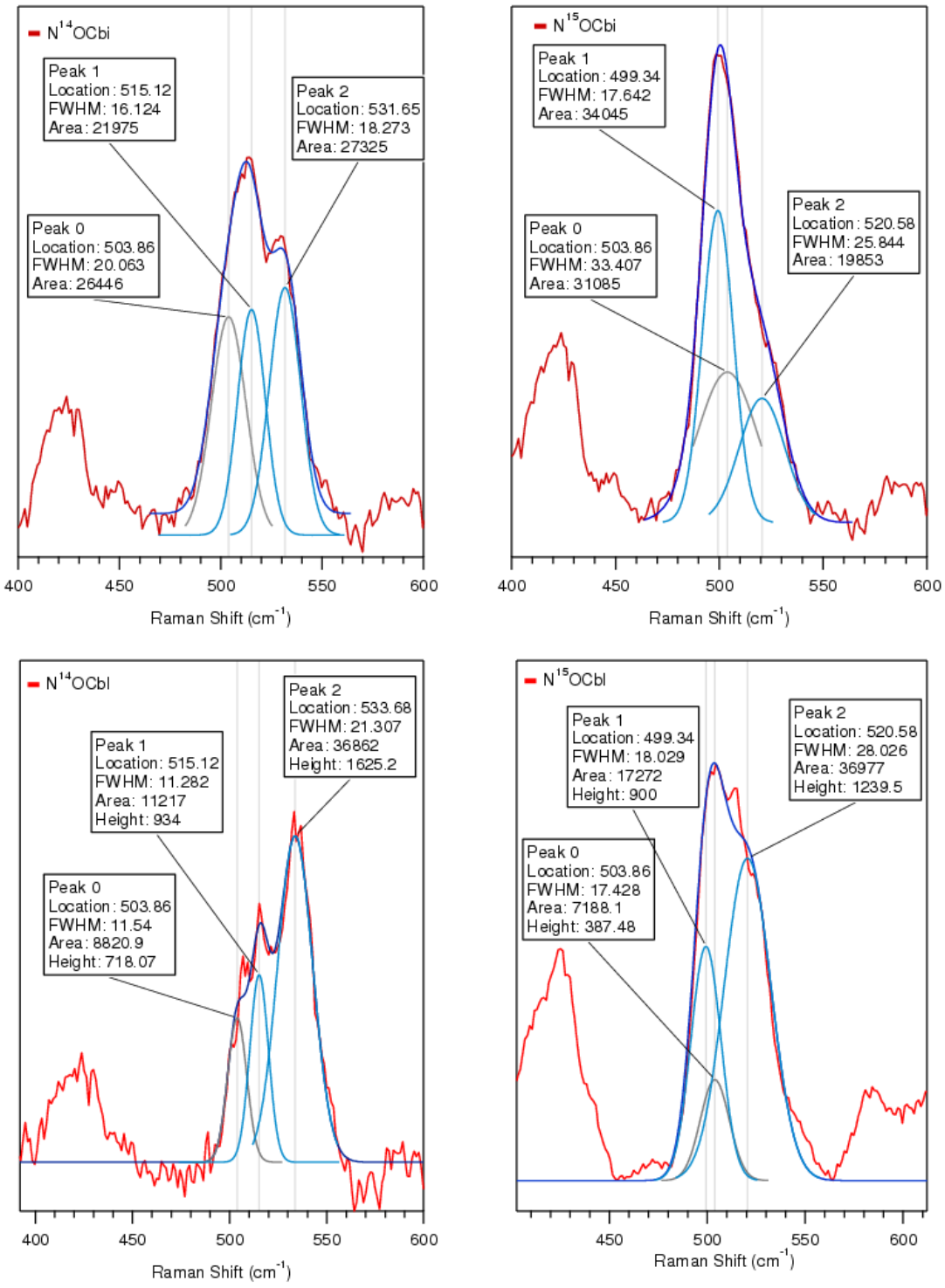

Figure S10: Gaussian deconvolution of the 77 K rR spectra of NOCbl, NOCbi$^+$, and their corresponding ^{15}NO-enriched spectra. Experimental traces are shown in red and fits are shown in dark blue. Individual isotope sensitive bands are shown in light blue, while the isotope-insensitive feature at ~504 cm^{-1} is shown in gray.

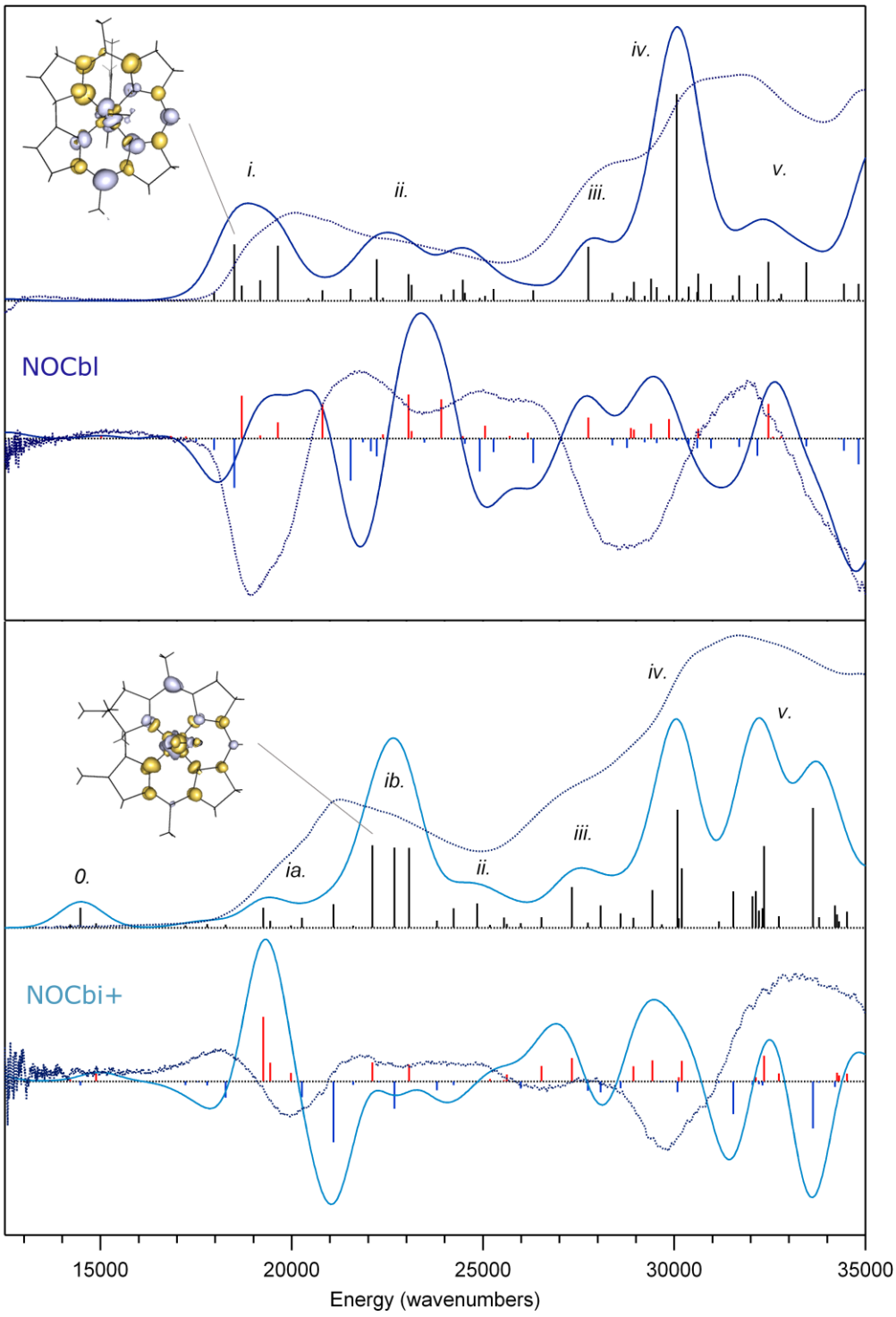

Figure S11: Abs and CD spectra of NOCbl (top) and NOCbi^{+} (bottom) collected at 4.5 K (in dotted lines) superimposed on the TDDFT results. The TDDFT transitions (vertical sticks) were convoluted with Gaussian bands, using a constant FWHM of 1,250 cm^{-1} to yield the solid traces (dark blue for NOCbl, and light blue for NOCbi^{+}). The EDDM for the α-band transition is shown on the left. Note the alternating regions of loss (gray) and gain (gold) of electron density. The calculated spectra were uniformly red-shifted by 2,200 cm^{-1} to facilitate a direct comparison with the experimental results.

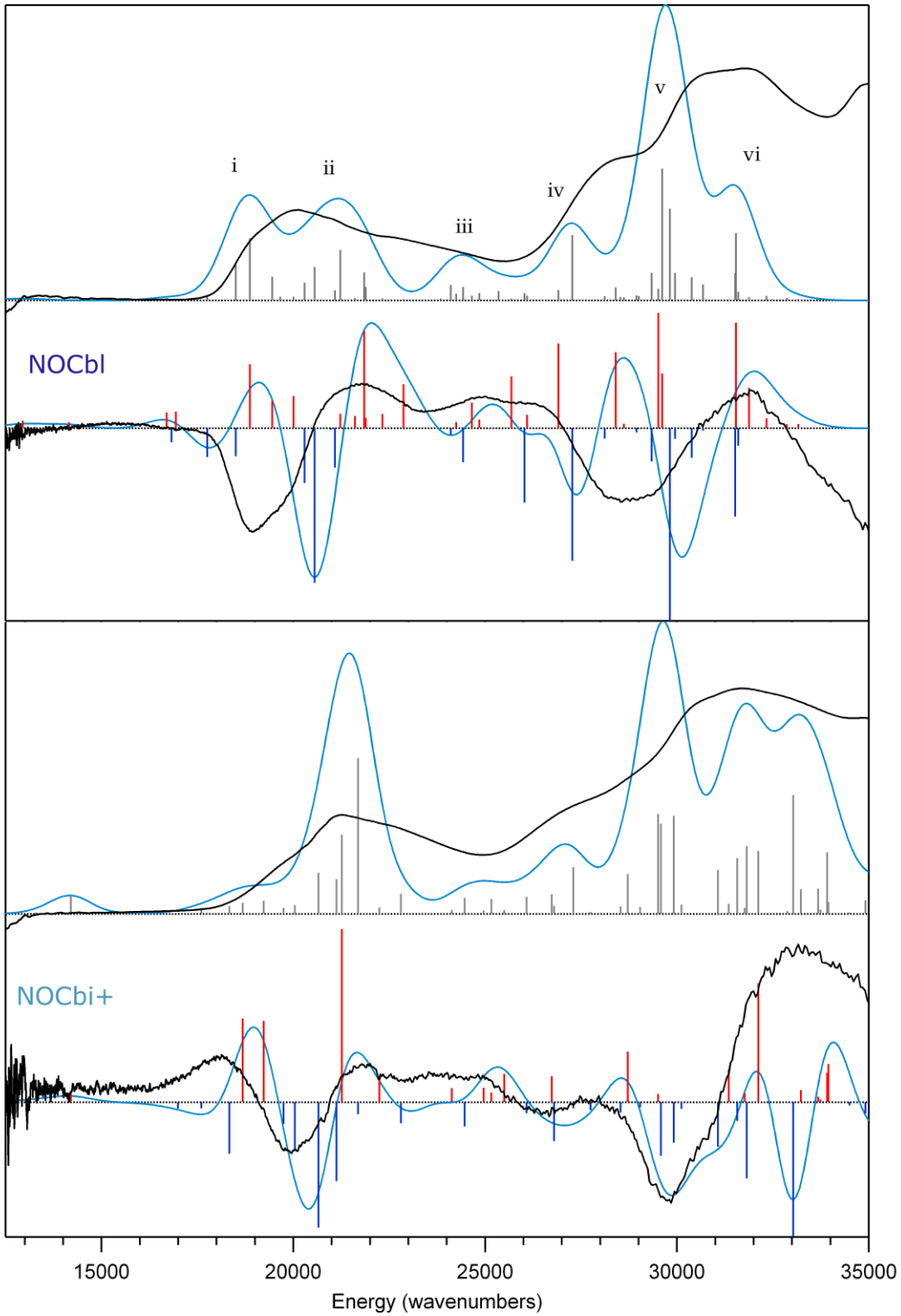

Figure S12: Abs and CD spectra of NOCbl (top) and $NOCbi^+$ (bottom) collected at 4.5 K (in black lines) superimposed on the TDDFT results for the truncated structural models of base-on (top) and base-off NOCbl (bottom) in blue lines. The TDDFT transitions (vertical sticks) were convoluted with Gaussian bands, using a constant FWHM of 1,250 cm^{-1} to yield the solid traces. The calculated spectra were uniformly red-shifted by 3,000 cm^{-1} to facilitate a direct comparison with the experimental results.

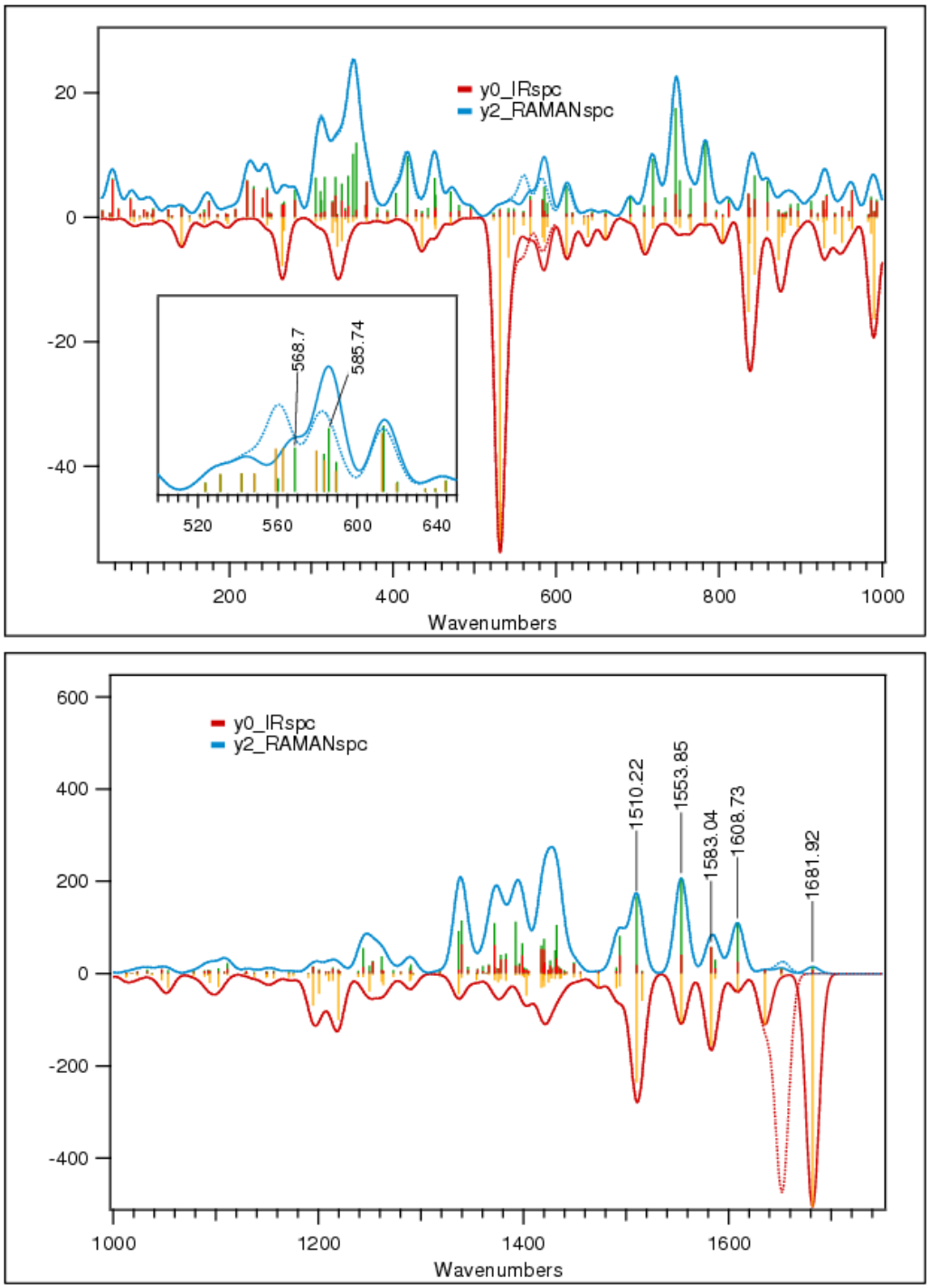

Figure S13: Calculated infrared (red traces, yellow sticks) and off-resonance Raman (blue traces, green sticks) spectra of NOCbl (solid lines) and ^{15}NOCbl (dotted lines). Top panel: low-energy region; bottom panel: high-energy region. Sticks indicate the individual transitions, which were convoluted with a 5 cm^{-1} Gaussian band to yield the spectral traces. The inset highlights the isotope-sensitive Co-NO modes. The depolarization ratios of the Raman transitions are shown by the red contributions to the individual sticks. No red indicates a depolarization ratio of 0, while fully red corresponds to a depolarization ration of 0.75.

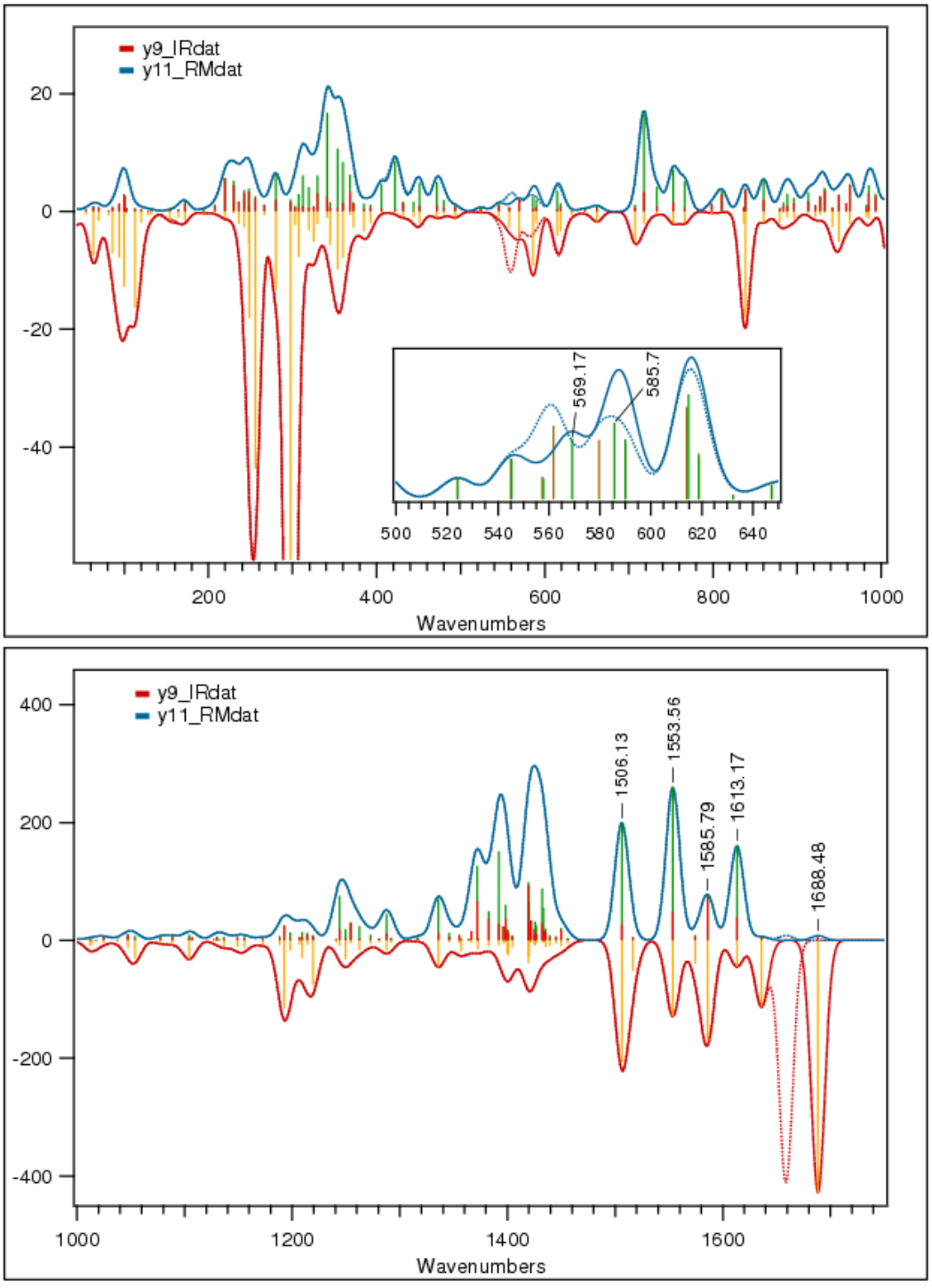

Figure S14: Calculated infrared (red traces, yellow sticks) and off-resonance Raman (blue traces, green sticks) spectra of $NOCbi^+$ (solid lines) and $^{15}NOCbi^+$ (dotted lines). Top panel: low-energy region; bottom panel: high-energy region. Sticks indicate the individual transitions, which were convoluted with a 5 cm^{-1} Gaussian band to yield the spectral traces. The inset highlights the isotope-sensitive Co-NO modes. The depolarization ratios of the Raman transitions are shown by the red contributions to the individual sticks. No red indicates a depolarization ratio of 0, while fully red corresponds to a depolarization ration of 0.75.

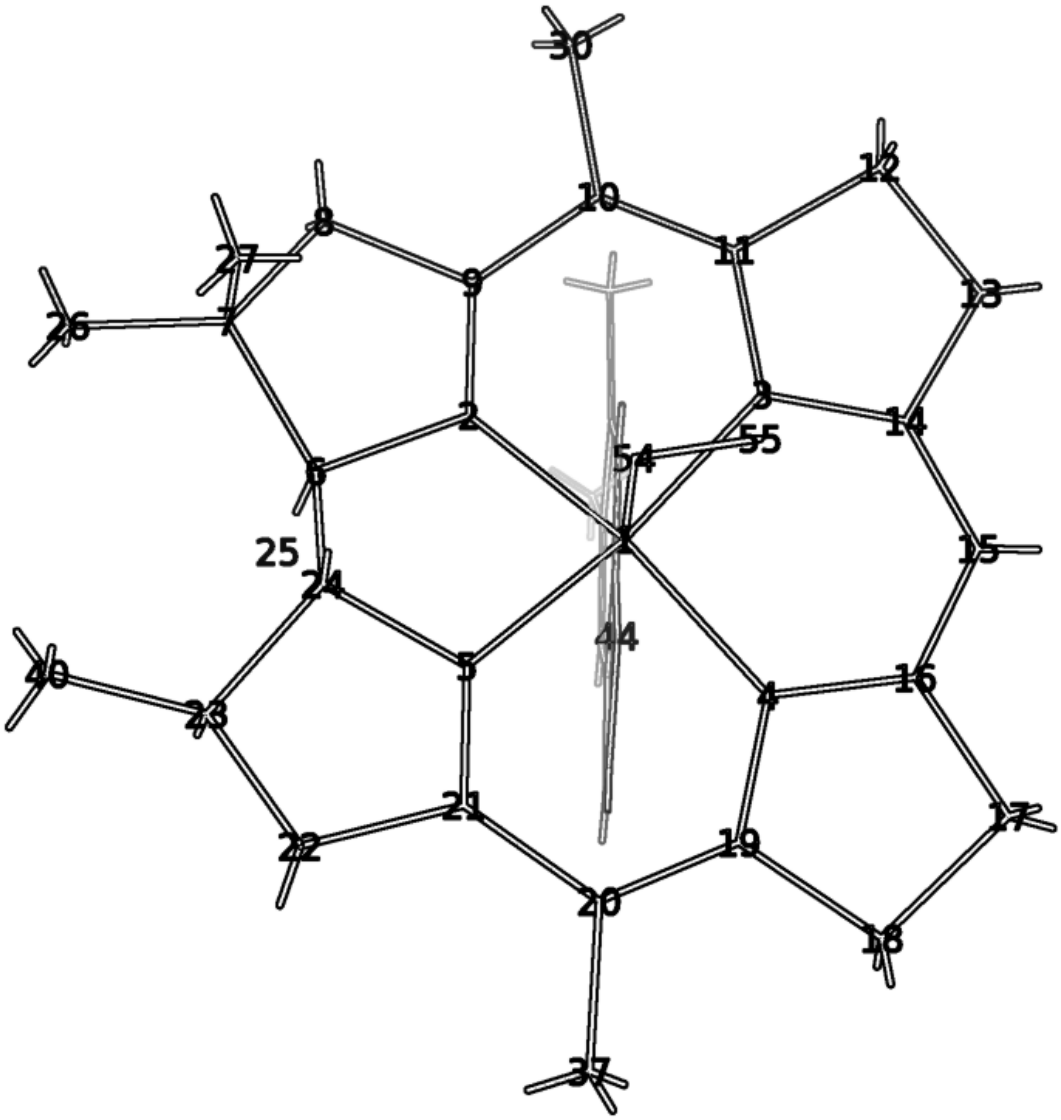

Figure S15. Truncated NOCbl model employed in this work showing the atom numbering scheme used in Table S1. Only the labels for non-hydrogen atoms of the corrin ring, the NO ligand, and the coordinating N atom of the DMB ligand are shown.

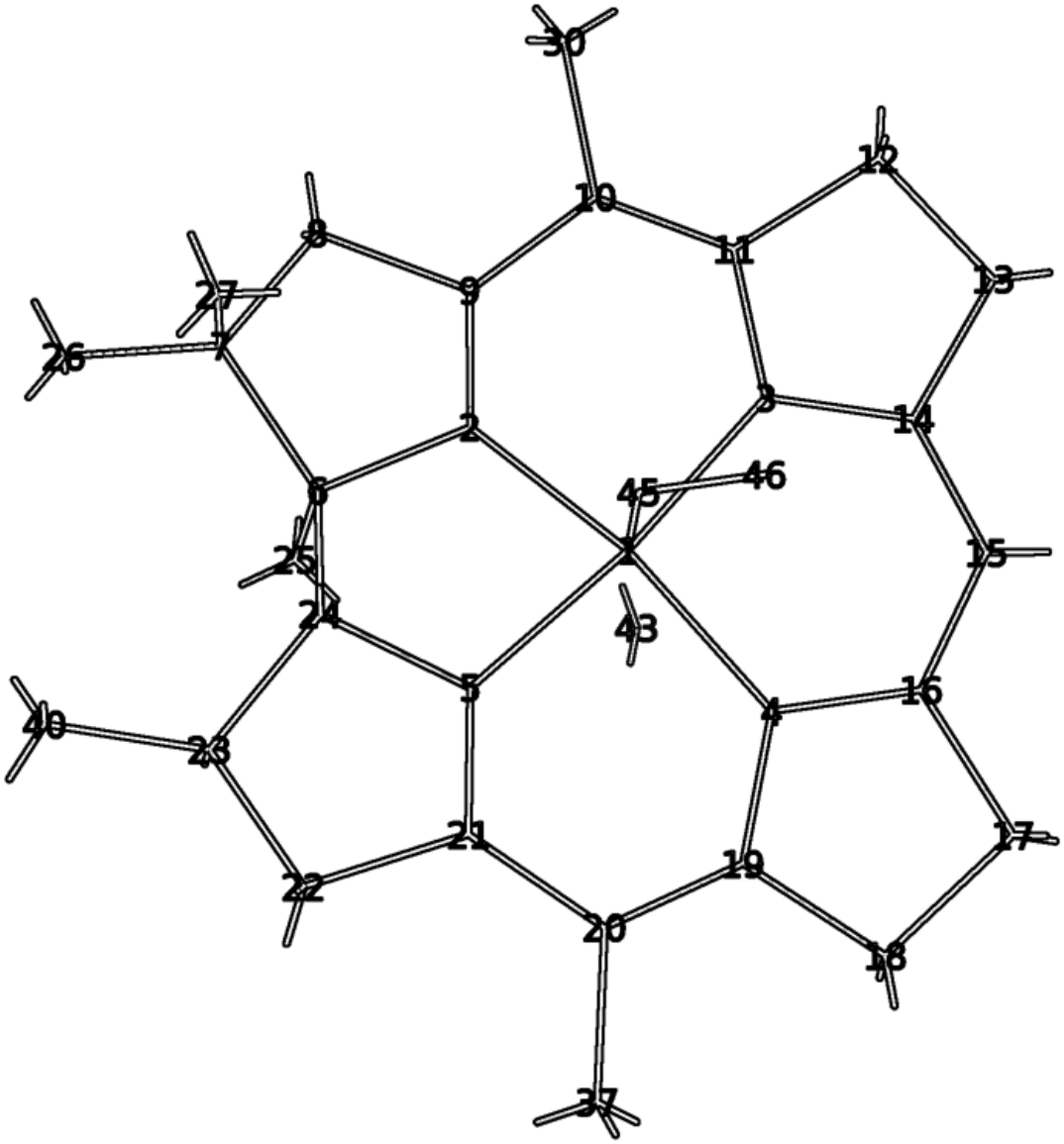

Figure S16. Truncated NOCbi^{+} model employed in this work showing the atom numbering scheme used in Table S2. Only the labels for non-hydrogen atoms of the corrin ring, the NO ligand, and the O atom of the water ligand are shown.

References

(1) Smith, A. T.; Majtan, T.; Freeman, K. M.; Su, Y.; Kraus, J. P.; Burstyn, J. N. *Inorganic Chemistry* **2011**, *50*, 4417.
(2) Weinhold, F.; Landis, C. L. *Valency and Bonding*; Cambridge University Press, 2005.